JACS
JOURNAL OF THE AMERICAN CHEMICAL SOCIETY

ARTICLE

pubs.acs.org/JACS

Tailoring Homochirality at Surfaces: Going Beyond Molecular Handedness

Matthew Forster,[†] Matthew S. Dyer,[†] Mats Persson,[†,‡] and Rasmita Raval[*,†]

[†]Surface Science Research Centre and Department of Chemistry, University of Liverpool, Oxford Street, Liverpool L69 3BX, U.K.
[‡]Department of Applied Physics, Chalmers University of Technology, SE-412 96 Göteborg, Sweden

ABSTRACT: Chirality can be bestowed upon a surface by the adsorption of molecules and is usually discussed in terms of the molecular handedness. However, the adsorption process often leads to a new manifestation of chirality in the form of the adsorption footprint, which can also be chiral and generate mirror-images in 2-D. Therefore, in describing the chirality of the interface, one must consider both the *handedness* and the adsorption '*footedness*' of the system. Specifically, the creation of a truly homochiral surface must ensure that a single chirality is expressed for each aspect, and requires not only the control of molecule handedness but also direct control over footedness. Here, we demonstrate the ability to engineer homochiral footedness by a structural modification of enantiopure (*S*)-proline, which normally creates a (4 × 2) organization on a Cu(110) surface with heterochiral footedness. This modification of proline via the addition of a double bond within the pyrrolidine ring, yielding 3-pyrroline-2-carboxylic acid (PCA), is sufficient to drive the footprints of the entire (4 × 2) assembly from heterochiral to homochiral, leading to the creation of a truly homochiral interface The effects of modifications upon the footprint arrangements were characterized at the single-molecule level by scanning tunnelling microscopy, reflection absorption infrared spectroscopy and periodic density functional theory calculations. The control of adsorption footprints is not only pivotal to tailoring chirality at surfaces but also plays a key role in dictating the organization, the outward facing functionalities and the response of the organic−inorganic interface.

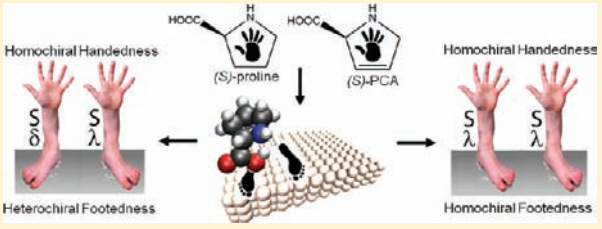

1. INTRODUCTION

The chirality of an interface, arising from the adsorption of molecules, has traditionally been described solely by the intrinsic handedness of the adsorbed molecule.[1−5] However, for molecules adsorbed at a surface a second manifestation of chirality may arise as a direct result of the molecule−substrate interaction. This interaction is described by the adsorption footprint, which considers the 2-D mesh enclosed by the bonding points of the molecule upon adsorption.[3] Interestingly, adsorption footprints may be chiral if they possess no reflectional symmetry elements, thus generating nonsuperimposable mirror images in 2-D.[6] Although, the concept of chiral adsorption footprints has already been used in the literature to describe the adsorption of both chiral[6−14] and achiral[6,8,9,15−17] molecules at surfaces, the overall description of the chirality of such organic−inorganic interfaces is often imprecise and blurs the contributions that arise from the molecule and from the adsorption footprint. Therefore, it was recently proposed by Mark et al.[18] that the chirality of an interface is more clearly expressed by explicitly considering both the *handedness* of the molecule and also the *footedness* of the adsorption complex, arising from footprint chirality. Essentially, footprint chirality introduces a new chiral center to the molecule-surface complex and a molecule with (*S*)- and (*R*)-handedness, and λ and δ footedness will have four possible stereoisomers as shown in Figure 1, (*S*)-λ, (*S*)-δ, (*R*)-λ, and (*R*)-δ. This handedness-footedness construction allows the manifestation of chirality at surfaces to be more clearly defined and deconvoluted. Most importantly, it raises the question, what is a truly homochiral interface? For example, we have previously demonstrated that an enantiopure molecule which generates a one-handed adlayer may also project heterochiral footprint arrangements.[19] Thus, it becomes clear that in order to create a truly homochiral interface

Figure 1. Handedness and footedness. The molecular handedness (enantiomers (*R*) and (*S*)) and adsorption footedness (δ and λ) combine to generate four diastereomers of the molecule−surface system.

Received: April 15, 2011
Published: September 01, 2011

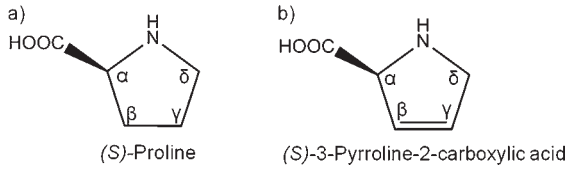

Figure 2. Molecular structure of (a) (*S*)-proline and (b) (*S*)-3-pyrroline-2-carboxylic acid (PCA).

it is necessary that both the *handedness* and *footedness* are of a single chirality.

An important and illustrative case is provided by the adsorption of amino-acids on metal surfaces, which has generated significant interest as a model system for exploring the expression of chirality in two-dimensional systems.[6−11,19−44] The complete structural characterization of these monolayers is demanding since it requires information, at the single-molecule level, on the molecular chirality, molecular conformation, and the adsorption footprints adopted within the organized assembly. This level of analysis was recently achieved by us for the (4 × 2) assembly of (*S*)-proline (Figure 2a) on Cu(110), where the individual conformation and footprint of each molecule may be mapped directly.[19] This work revealed that an enantiopure molecule which generates a one-handed adlayer actually projects a heterochiral adsorption footprint arrangement at the interface. Specifically, the ability to map the individual footprints of the (*S*)-proline (4 × 2) organization presented a unique opportunity to examine and demonstrate whether the chirality of such an interface can be advanced toward complete homochirality via control of footedness.

Here, we show for the first time, that footprints within a surface organization may be driven to adopt a single chirality by engineering targeted structural modification of the molecule. This enables the system to achieve homochirality at the footedness level in addition to homochirality at the handedness level, thus creating a truly homochiral interface. In addition, experimental detail obtained at the single-molecule level, allied with theoretical modeling, provide molecular-level insights into the mechanism of how the chirality of a surface assembly may be tailored to design. Specifically, we show that the modification of (*S*)-proline by the addition of a double bond within the pyrrolidine ring between the β and γ carbon positions, yielding (*S*)-3-pyrroline-2-carboxylic acid (PCA, Figure 2b) directly influences the footprints adopted upon deposition on a Cu(110) surface. Results from scanning tunnelling microscopy (STM), low-energy electron diffraction (LEED), reflection absorption infrared spectroscopy (RAIRS), and periodic density functional theory calculations (DFT) demonstrate that this subtle structural alteration is sufficient to promote a (4 × 2) organization which contains a single conformer species and leads to the projection of a truly homochiral footprint assembly. This is in direct contrast to the heterochiral footprint assembly observed for the (4 × 2) organization of (*S*)-proline on Cu(110).[19] Thus, this work shows that engineering the chirality of a molecule−surface system can now be advanced beyond the control of molecular handedness to control of adsorption footedness of an interface by careful consideration of molecular structure in order to create a truly homochiral interface.

We note that homochiral surfaces are of fundamental importance with potential applications envisaged in sensors,[45] enantioselective catalysis,[46] molecular electronics and devices,[47,48] and nonlinear optical materials[49−52] and the ability to elicit a truly chiral response may require engineering of both the handedness and footedness of the interface. In a broader context, the control of molecular footprints has other important ramifications. For example, the molecular footprint is essential for providing a full description of an interface, since the footprint determines both the orientation and positioning of the functional groups of a molecule on a surface. Thus, footprints directly influence the response of adsorbed molecular layers with their local environment.[53] Furthermore, it has recently been shown that footprints dictate the way in which molecules organize on surfaces. For example, the chiral organization and chiral recognition of amino-acids and bicarboxylic acids at surfaces is determined to a large extent by the footprint arrangement.[1,20,21,53,54] Finally, adsorption footprints are of central importance in ligand protected nanoparticles where the 'chiral footprint model' has been intimately linked to the origin of optical activity in metal-based electronic transitions.[49−52]

2. METHODS

The Cu(110) surface was prepared by Ar^+ sputtering at 500 eV followed by annealing to 800 K. (*S*)-PCA (99%, Sigma Aldrich) was dosed from an electrically heated glass tube, with the Cu crystal at room temperature. STM images were recorded in an ultra-high vacuum chamber, with a base pressure of 2×10^{-10} mbar, fitted with a Specs Aarhus 150 STM operated in constant current mode with an electrochemically etched tungsten tip. RAIRS experiments were performed in a UHV chamber interfaced with a Mattson 6020 FTIR spectrometer via ancillary optics and KBr windows. A nitrogen-cooled HgCdTe detector allowed the spectral range of 650−4000 cm^{-1} to be accessed. The resolution of the spectrometer was set to 4 cm^{-1}, and 250 scans were coadded. The spectrum of the clean sample was taken as a background reference, R^0, at the beginning of the experiments. Spectra of the adsorbed layer were then obtained during continuous dosing and are displayed as the ratio $(R - R^0)/R^0$ with respect to the clean sample spectrum.

Periodic DFT calculations were carried out using the VASP periodic density functional theory (DFT) package.[55] Plane waves were used as a basis set with an energy cutoff of 400 eV. Valence electron−core interactions were included using the projector augmented wave method,[56] and the generalized gradient approximation was used for the exchange-correlation functional.[57] The Cu(110) surface was included as a six-layer slab. Calculations of isolated PCA anions on this surface were carried out in a supercell corresponding to a (4 × 4) surface unit cell and a total height of 20.6 Å and were performed on a 4 × 3 × 1 *k*-point grid. Calculations of the (4 × 2) arrangements were carried out in a smaller supercell containing two anions in a (4 × 2) surface unit cell, but with the same height, and were performed on a 4 × 6 × 1 *k*-point grid.

In every case geometry relaxation was performed on the PCA anions and the top three copper layers until the force on every atom was smaller than 0.01 eV/Å. Corrections were made to the energy and electrostatic potential to compensate for periodic images of the dipole moment in the *z*-direction. In-spite of the fact that the adsorbed PCA species is formally anionic the calculations were performed in a cell without an overall charge. Charging occurs by transfer of electrons from the metal surface to the dehydrogenated PCA molecule, accompanied by a compensating screening charge within the metal substrate. Following geometry relaxation the adsorption energy was calculated in the (4 × 4) supercell by comparing to the energies of a hydrogen atom adsorbed at the short bridge site, a PCA molecule in vacuum and a clean copper surface calculated in the same supercell.

Since the calculated energy differences between different adsorbed conformers and arrangements of molecules on the surface are likely to be

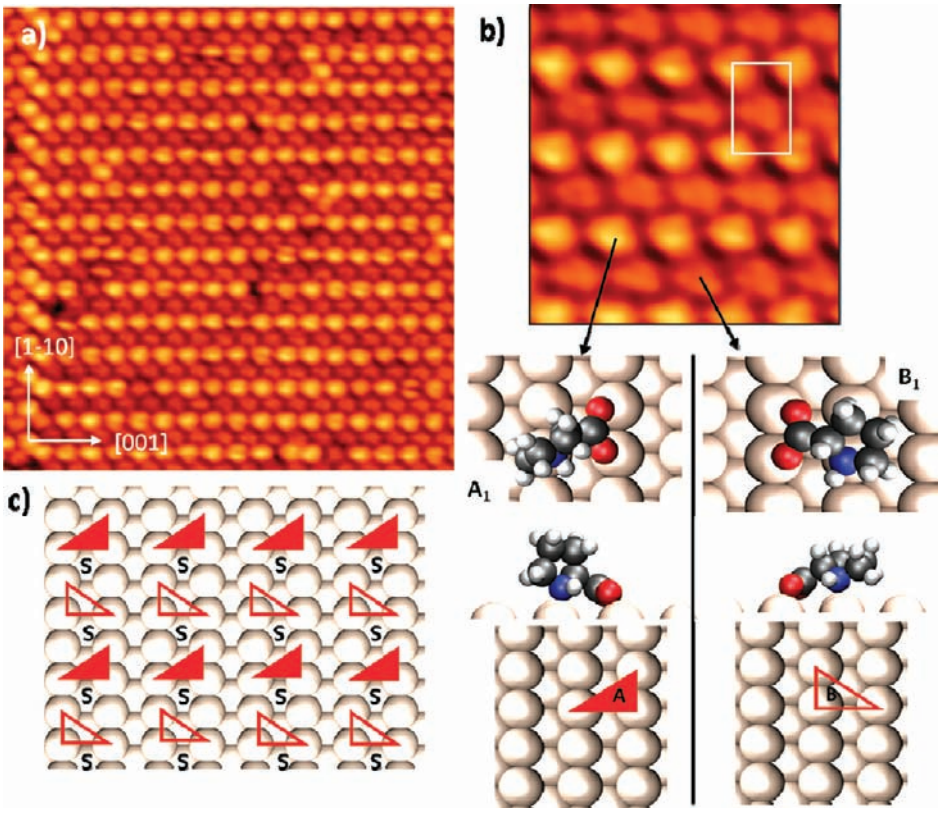

Figure 3. (a) STM image of the (4 × 2) structure of (*S*)-proline on Cu(110) (140 × 128 Å^2, I_t = −0.40 nA, V_t = −806 mV). (b) Expansion STM image (37 × 39 Å^2, I_t = −0.47 nA, V_t = −423 mV) showing the (4 × 2) unit containing two distinct conformers (A and B). For each conformer black arrows indicate the DFT optimized geometry, shown from above and the side (color code: red = oxygen, blue = nitrogen, black = carbon, white = hydrogen), and corresponding adsorption footprint. (c) Schematic representation of the heterochiral adsorption footprint arrangement for the (4 × 2) prolate structure (filled triangles = conformer A, open triangles = conformer B). Figure adapted from ref 19.

small and toward the limit of DFT reliability, we have also simulated the results of STM and RAIRS experiments for our models, in order to add support in the case where an argument on the basis of energy alone may be insufficient. Constant current STM images were simulated in the Tersoff−Hamann approximation,[58] by plotting contours of constant integrated local density of states (LDOS) from the Fermi energy to the bias potential. It is not possible to obtain absolute values of the tunneling currents at a given tip−surface height using the Tersoff−Hamann approximation, so the LDOS plots in this study are shown with an average tip−surface distance of 7.5 Å. This is large enough to avoid the region in which there would be a chemical interaction between the tip and the sample, which is not included in this method. In addition, this tip−surface distance was utilized for the (*S*)-proline on Cu(110) study and yielded STM simulations that were representative of experiment.[19]

The normal modes for the adsorbed species were calculated in the harmonic approximation. In the calculation of the normal modes the top layer of the copper surface was included in addition to the (*S*)-PCA anions, with the remaining copper atoms kept fixed. At the same time, the change in the dipole moment in the *z*-direction was calculated for each mode and used to simulate the results of RAIRS experiments. It should be noted that DFT calculated normal-mode frequencies are only accurate to within approximately 50 cm^{-1} but are sufficient for a meaningful comparison with experiments.[59]

3. RESULTS AND DISCUSSION

3.1. Homochiral Handedness and Heterochiral Footedness: The (4 × 2) Assembly of (*S*)-Proline on Cu(110).

We have recently shown that within the (4 × 2) overlayer of (*S*)-proline on Cu(110), two distinct anionic prolate conformers are present which image as bright and faint protrusions in STM (Figure 3a,b).[19] The two conformers arise as a direct consequence of two possible adsorption footprints that can be adopted. Both conformers bond to the surface through the two oxygen atoms of the carboxylate which bind to two adjacent copper atoms along the close packed row. The third bonding contact is via the nitrogen to one of the copper atoms directly opposite in the neighboring row. The two conformers differ in terms of which copper atom the nitrogen of the NH group interacts with. Since, the NH group is incorporated within the pyrrolidine ring, this essentially forces the ring to track the nitrogen position and adopt different orientations as the nitrogen moves to a particular bonding position. Thus, if the nitrogen bonds to the copper atom that lies to the left, a left-handed triangular footprint is described, and the pyrrolidine ring is forced to tilt significantly away from the surface (conformer A_1, Figure 3b), imaging as a bright protrusion in STM. If, however, the nitrogen bonds to the right, a right-handed triangular footprint is described, and the ring is forced to lie flat (conformer B_1, Figure 3b) and images as a faint protrusion. Thus, the chirality of the (4 × 2) monolayer is expressed in an interesting manner. On the one hand, the enantiopure adsorbate leads to a *homochiral* molecular layer. However, both left- and right-handed adsorption footprints are adopted leading to a *heterochiral* footprint arrangement (Figure 3c).[19]

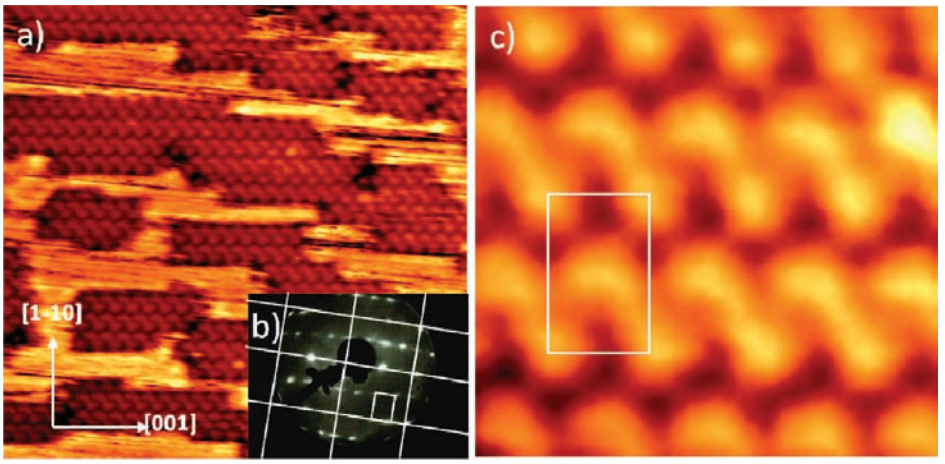

Figure 4. (a) STM image showing the (4 × 2) organization of (*S*)-PCA (165 × 179 Å^2, I_t = −0.37 nA, V_t = −1250 mV). (b) LEED image showing the (4 × 2) organization of (*S*)-PCA on Cu(110) collected at 72 eV with grid from the primary Cu (1 × 1) spots overlaid. (c) High-resolution STM image of the (4 × 2) PCA assembly (38 × 40 Å^2, collected under same tunneling conditions as used for (a)).

3.2. Homochiral Handedness and Homochiral Footedness: (*S*)-PCA on Cu(110). *3.2.1. STM Investigation of (S)-PCA on Cu(110): The (4 × 2) Assembly.* In order to tailor the adsorption footprints adopted within amino-acid overlayers so that complete homochirality can be expressed at both the handedness and footedness levels, we turned to the proline derivative (*S*)-PCA which retains the important functional units of proline in terms of the footprint (the carboxylic acid and amino groups) but contains a subtle structural modification in the form of a double bond within the pyrrolidine ring, Figure 2b. Most importantly, the NH group remains incorporated within the pyrrolidine structure so that the ring position and orientation are directly affected by the bonding site adopted by the NH group, thus acting as a marker for footprint geometry, in a directly analogous manner to (*S*)-proline on Cu(110),[19] as discussed in the previous section.

Like proline, PCA adsorbs on the Cu(110) surface in its anionic form, as shown by RAIRS data which will be discussed in detail later (section 3.2.4). STM and LEED images show adsorption of (*S*)-PCA on Cu(110) at 300 K leads to a (4 × 2) overlayer (Figure 4a−c), analogous to the organization of (*S*)-proline on the same surface (Figure 3).[19] The incorporation of an unsaturated bond within the pyrrolidine ring, therefore, does not alter the surface ordering. Examination of high resolution STM images of the (*S*)-PCA overlayer (Figure 4a,c) shows that molecules image as pairs with a diagonal top-left to bottom-right alignment, which we will hereafter refer to as left-handed dimers. Furthermore, there is no contrast in the apparent height of molecules within the overlayer, unlike the (*S*)-proline (4 × 2) structure which contains two distinct conformers that image differently (conformers A_1 and B_1, Figure 3b). The apparent height of the (*S*)-PCA protrusions is equivalent to those of the 'faint' imaging protrusions of the (*S*)-proline system (conformer B_1, Figure 3b), suggesting that the (4 × 2) (*S*)-PCA overlayer contains a single, flat ring conformer species.

3.2.2. DFT Investigation of (S)-PCA on Cu(110): The Isolated Species. In order to gain further insight into the differences between the (*S*)-PCA and (*S*)-proline (4 × 2) overlayers periodic DFT calculations were undertaken. Calculations were initially performed for the adsorption of an isolated (*S*)-PCA anion. The two most stable geometries identified (conformers A_2 and B_2) are shown in Figure 5 and are analogous to the two most stable conformers identified for the (*S*)-proline system (conformers A_1 and B_1, Figure 3b),[19] which possess mirror-image (chiral) triangular adsorption footprints. Conformer A_2 has a tilted pyrrolidine ring geometry and is described by a left-handed footprint, whereas conformer B_2 has a right-handed footprint and possesses a flat ring geometry. The calculated adsorption energies of conformers A_2 and B_2 are 1.18 and 1.22 eV per molecule, respectively, showing that the flat ring conformer enjoys only a slight energetic preference compared to its tilted counterpart.

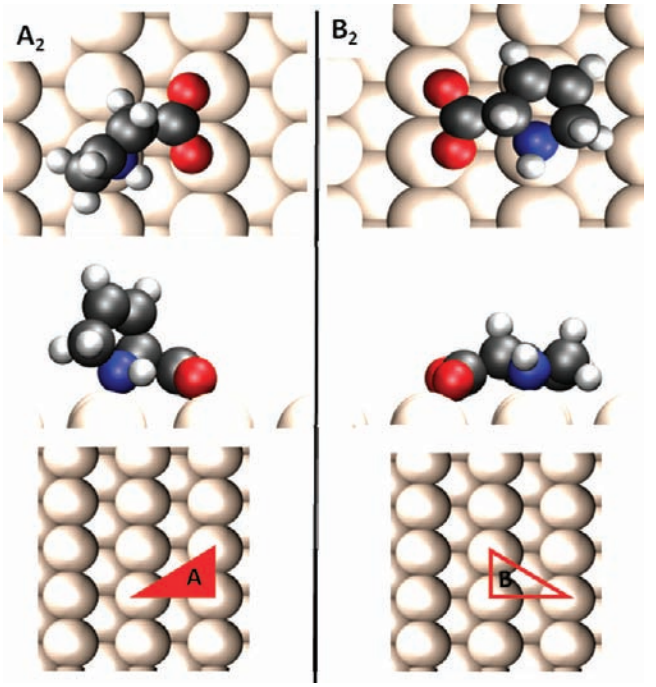

Figure 5. Relaxed adsorption geometries of the two most stable isolated (*S*)-PCA anions (conformer A_2 and B_2) in a (4 × 4) unit cell on Cu(110), shown from above, from along the close-packed rows and in terms of the molecular adsorption footprint (color code for atoms as defined in Figure 3).

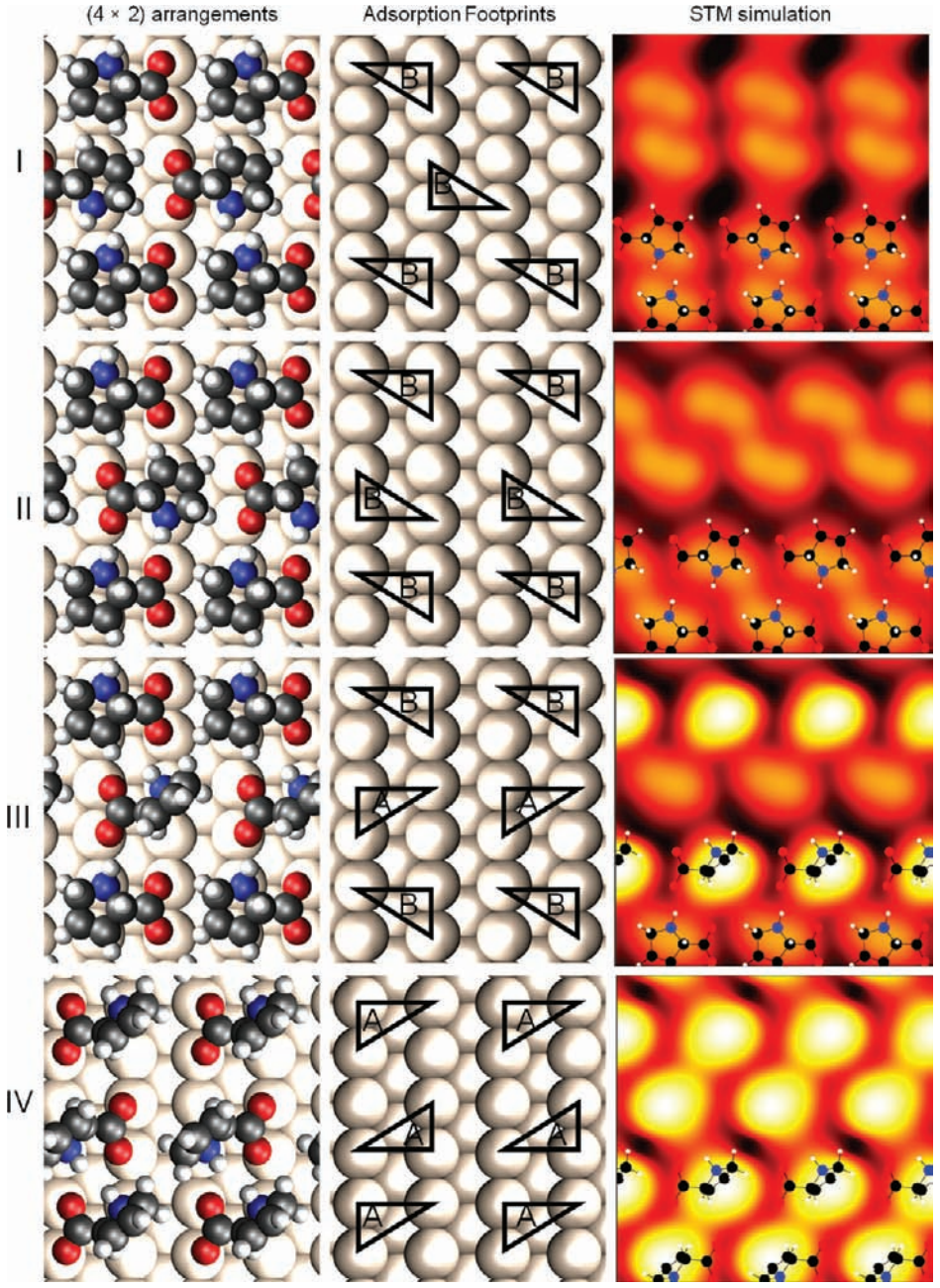

Figure 6. Relaxed adsorption geometries, adsorption footprints arrangements, STM simulations for the (4 × 2) arrangements I, II, III, and IV of (*S*)-PCA on Cu(110). Color code for atoms is as in Figure 3. Calculated STM images are shown in a (8 × 6) surface unit cell and are simulated at a bias voltage of −1.25 V with an average tip−surface height of 7.5 Å.

In the (*S*)-proline system the tilted ring conformer (conformer A_1, Figure 3b) was the more stable species,[19] suggesting the inclusion of a double bond within the pyrrolidine ring acts to stabilize molecules with a flat ring geometry. This is supported by the calculations which suggest that the C═C double bond of conformer B_2 interacts with the surface, providing an additional binding site. As a result, there is an increase in the calculated C═C bond length from 1.34 Å for conformer A_2 to 1.36 Å for conformer B_2. In addition, the calculated Cu−C bond lengths from the double bond of conformer B_2 are 2.29 and 2.36 Å. These bond lengths are similar to the calculated C═C and Cu−C bond lengths for the adsorption of π-bonded ethylene on Cu(110),[60,61] providing further support for the interaction of the double bond with the surface. Therefore, simply by the inclusion of a double bond within the pyrrolidine ring we have been able to reverse the stability of the isolated molecule from the proline system, where conformer A_1 was more stable by 30 meV, to conformer B_2 for PCA, which is favored by 40 meV.

3.2.3. DFT Investigation of (S)-PCA on Cu(110): The (4 × 2) Assembly. It is now important to consider how PCA molecules are arranged within the (4 × 2) assembly. Although experimental STM images (Figure 4a,c) suggest that the organization contains a single conformer species, DFT calculations identify two energetically similar (*S*)-PCA conformers with flat and tilted ring geometries (Figure 5). Therefore, models of (4 × 2) arrangements containing combinations of conformer A_2 and/or B_2 were

considered. There are eight possible (4 × 2) arrangements that can be constructed using both conformers A_2 and B_2; however, we limited our search to the four most favorable arrangements identified in the (*S*)-proline study.[19] The four candidate arrangements (I, II, III and IV) are shown in Figure 6 with the respective calculated adsorption energy per molecule reported in Table 1. Arrangements I and II are composed using only conformer B_2 and, therefore, both possess footprint homochirality. Two distinct orientations (rotamers) of the adsorption footprint are utilized, related by a 180° rotation, and the models differ only in the placement of the central molecule within the (4 × 2) unit. Arrangement III is directly analogous to the (4 × 2) structure of (*S*)-proline on Cu(110) and contains a 50:50 mixture of conformers A_2 and B_2 in a heterochiral adsorption footprint arrangement. Arrangement IV is constructed using conformer A_2 only and also possesses footprint homochirality. For each of the (4 × 2) arrangements an STM image was simulated for direct comparison with experiment (Figure 6). From this comparison it is clear that only arrangement II provides agreement with experiment (Figure 7), in which there is a left-handed dimer motif and no height contrast between the protrusions of each molecule. In addition, arrangement II also possesses the most favorable adsorption energy of all models considered.

3.2.4. RAIRS Study of (S)-PCA on Cu(110): Theory vs Experiment. Additional evidence for the creation of a single conformer (*S*)-PCA assembly is provided by RAIRS. The experimental spectrum collected for the (4 × 2) layer is shown in Figure 8 along with the calculated RAIR spectrum for isolated conformers A_2 and B_2 and the energetically preferred (4 × 2) structure (arrangement II, Figure 6) on the Cu(110) surface. It is apparent that the experimental spectrum and the simulated spectrum of both the isolated conformer B_2 and arrangement II are in good agreement, reproducing the correct spectral pattern containing the major peaks at the approximately correct intensity, whereas the simulated spectrum for conformer A_2 does not agree with experiment. This observation adds further support to the creation of a (4 × 2) overlayer containing only conformer B_2. The calculated modes for the (*S*)-PCA spectra show significant intermixing of vibrational bands; however, a broad comparison between experiment and theoretical assignments of the major spectral regions is attempted below.

Table 1. Adsorption Energies (E_{ads} in eV/molecule) of (4 × 2) Arrangements of (*S*)-PCA Anions on Cu(110)[a]

arrangement	I (B_2)	II (B_2)	III (A_2 + B_2)	IV (A_2)
E_{ads}	0.87	1.34	1.32	1.25

[a] The conformers (A_2 and/or B_2) contained within each arrangement are stated.

For the CH_2 stretching region an intense double peak at 2798 and 2777 cm^{-1} in the experimental spectrum is reproduced by the simulated spectrum for arrangement II at 2837 and 2804−2799 cm^{-1}, respectively. Calculations show that it is the $C_\delta H_2$ symmetric stretch and the $C_\alpha H$ stretch which give rise to peaks in this region. This is consistent with previous calculations for the (*S*)-proline system where the same stretching modes from the conformer with the flat lying ring (conformer B_1, Figure 3b) gave rise to intense peaks in the RAIR spectrum.[19] The peak with medium intensity at 1421 cm^{-1} in the experimental spectrum is assigned to the symmetric carboxylate stretch mode. The absence of the corresponding asymmetric stretch suggests both oxygen atoms of the carboxylate are equidistant to the surface, consistent with previous examples of amino acids on Cu(110).[19,29−37] The symmetric stretching mode is reproduced in the simulated spectrum of arrangement II at 1385 cm^{-1} and is coupled to the NH in-plane bend and CH deformations. The NH bond of conformer B_2 lies broadly parallel to the surface, leading to only medium intensities for the normally intense NH bends. Calculations show that the main contributions from the in-plane NH bends occur at 1385, 1290, and 1191 cm^{-1} corresponding to peaks at 1421 and 1274 cm^{-1} in the experimental spectrum. The out-of-plane NH bends occur at 1011 and 980−941 cm^{-1} which are also in agreement with experiment with peaks located at 1030 and 960 cm^{-1}.

3.3.5. Heterochiral vs Homochiral Footprint Arrangements: The Driving Forces. Results from both experiment and theory show that the (*S*)-PCA (4 × 2) assembly consists of a single conformer species possessing a flat ring geometry. This species consists of an adsorption footprint of a single chirality which is arranged within the assembly in two distinct rotamer states (arrangement II, Figure 6), creating a *homochiral* footprint arrangement. This is in direct contrast to the (4 × 2) organization of (*S*)-proline which utilizes two conformers A_1 and B_1 in equal measure, which project left- and right-handed footprints and, therefore, generates a *heterochiral* footprint arrangement.[19] Previous theoretical studies for other amino-acid overlayers also

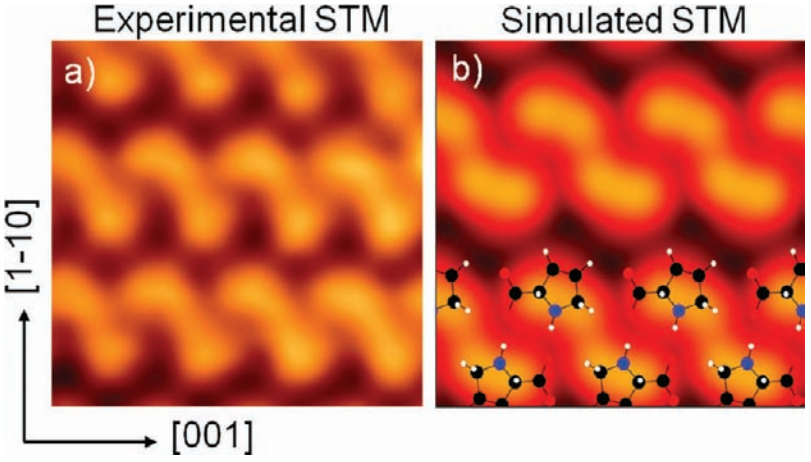

Figure 7. (a) High resolution STM image of the (4 × 2) structure of (*S*)-PCA on Cu(110) (30 × 29 Å^2, I_t = −0.37 nA, V_t = −1250 mV). (b) Simulated STM image of arrangement II under the conditions described in Figure 6; the positions of the molecules are included.

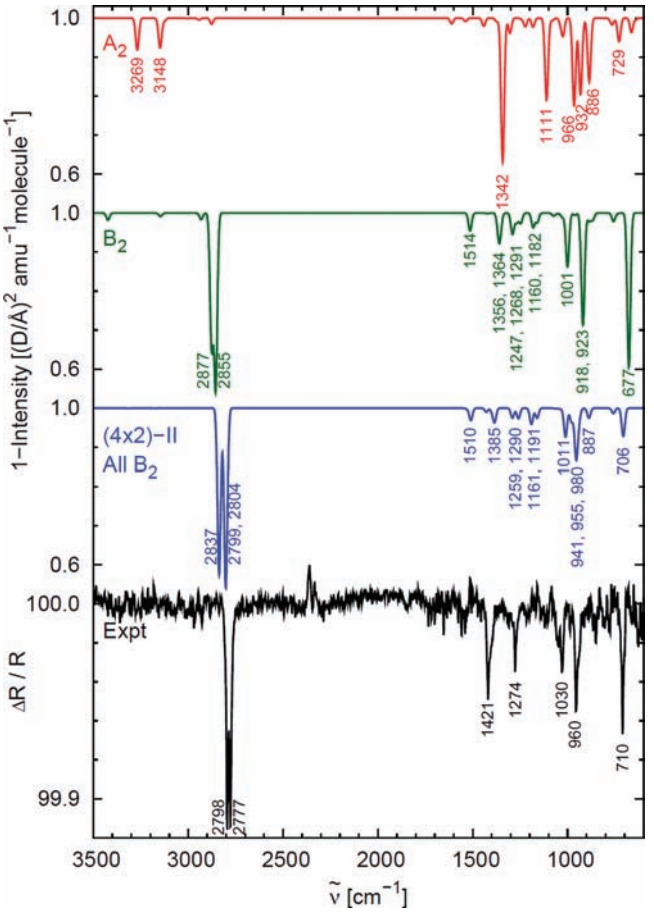

Figure 8. Spectra from top to bottom: Simulated RAIR spectrum for an isolated (*S*)-PCA anion of conformer A_2 (red) and conformer B_2 (green), simulated RAIR spectrum for arrangement II (blue) containing only the B_2 species and experimental RAIR spectrum for the high coverage adsorption of (*S*)-PCA on Cu(110) (black).

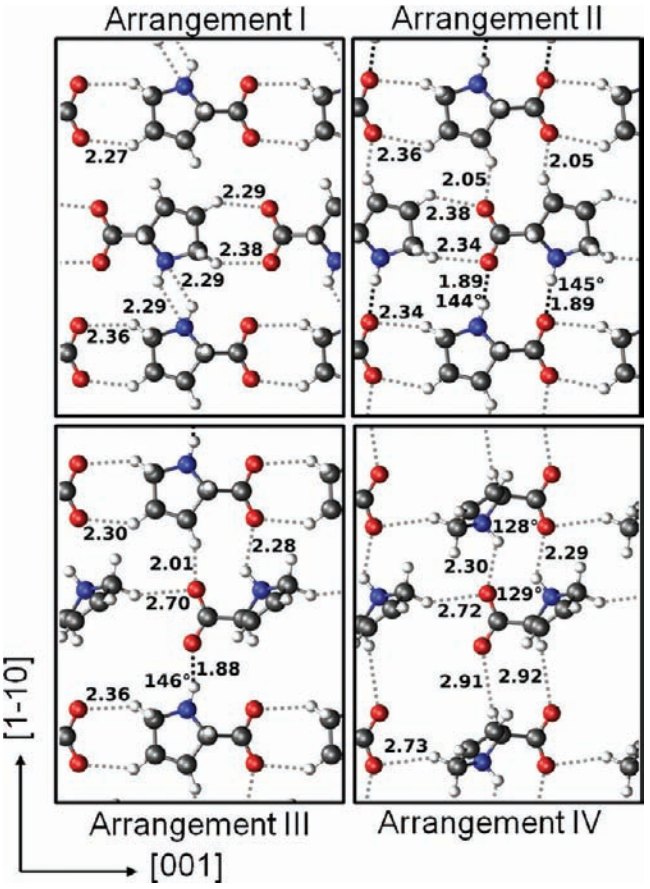

Figure 9. Potential hydrogen-bonding interactions for arrangements I, II, III, and IV. Strong hydrogen bonds are indicated by black dashes, weaker bonds by gray dashes. Bond lengths and angles are indicated. We define a strong hydrogen bond as the interaction between nitrogen/oxygen and hydrogen at a distance of 2 Å or less. Color code for atoms is as in Figure 3.

predicted the adoption of *heterochiral* adsorption footprints arrangements.[8−10] In contrast, this work shows that it is possible to force the projection of a *homochiral* footprint arrangement at an interface via targeted structural modification of the adsorbed molecule.

Let us now consider the driving forces that define whether an assembly adopts a heterochiral or a homochiral footprint arrangement. The intermolecular hydrogen-bonding interactions for each of the proposed (*S*)-PCA (4 × 2) arrangements are presented in Figure 9. Arrangement II, which provides excellent agreement with experiment, is shown to generate hydrogen-bonded dimers, each sustaining two strong hydrogen bonds[62] with a distance of 1.89 Å at angles of 144° and 145°. In addition, arrangement II avoids an energy penalty associated with induced compressive strain when adjacent carboxylate groups bond to every copper atom in a close packed row.[21] This strain is avoided by the single PCA conformer occupying two distinct orientations that are related by a 180° rotation (Figure 6). Arrangement I also generates hydrogen bonded dimers, however, a highly unfavorable adsorption energy (Table 1) is computed as a result of compressive strain. Arrangement III sustains 1-D hydrogen-bonded chains in the same manner as (*S*)-proline[19] and possesses a favorable adsorption energy (Table 1); however, the simulated STM image provides poor agreement with experiment. Finally, arrangement IV possesses the weakest hydrogen-bonding interactions and produces an STM simulation in poor agreement with experiment. Furthermore, the presence of A_2 conformers in arrangements III and IV are not supported by the comparison of simulated RAIR spectra with experiments. Thus, overall, arrangement II possesses the highest calculated adsorption energy (Table 1), an STM simulation and RAIR spectrum in excellent agreement with experiments and creates a strong hydrogen-bonding arrangement. The addition of a double bond within the pyrrolidine ring for PCA provides a fourth bonding point to the surface and thus stabilizes conformer B_2 relative to conformer A_2. This preference is sufficient to ensure the (*S*)-PCA (4 × 2) organization adopts a single conformer, homochiral footprint assembly and demonstrates the subtle balance between the molecule−substrate and molecule−molecule interactions, which ultimately define molecular organization at surfaces.

4. CONCLUSIONS

In conclusion, we have demonstrated, using a combined STM, RAIRS, and periodic DFT study, that it is possible to tailor the chirality of a surface by controlling not only the molecular *handedness* but also the adsorption *footedness*. In this work the adsorption footprints adopted within amino acid monolayers were engineered

by targeted structural modifications. Utilizing the single-molecule analysis afforded by the (4 × 2) assembly of (*S*)-proline on Cu(110) we show that inclusion of a double bond within the pyrrolidine ring promotes the stability of one particular chiral footprint in contrast to the two favored by proline. The preferred (*S*)-PCA conformer possesses a flat ring geometry as a direct result of the double bond, and this interaction is sufficient to promote the stability of a flat ring conformation relative to a tilted ring geometry in which the double bond cannot interact with the surface. Overall, this leads to the projection of a truly *homochiral* footprint assembly, in contrast to the *heterochiral* footprint arrangement favored by (*S*)-proline and a number of other amino acids on the Cu(110) substrate.[8−10,19,29−37] Thus, (*S*)-PCA represents a truly homochiral surface in which both the handedness and the footedness are of a single chirality. Finally, footprint arrangements dictate the molecular conformations adopted at the surface, which govern the outward-facing functionalities of the adlayer and thus the response of the interface. Therefore, the ability to identify and tune the adsorption footprints of organized assemblies represents an important advance in the control and manipulation of molecular interfaces.

AUTHOR INFORMATION

Corresponding Author
R.Raval@liv.ac.uk

ACKNOWLEDGMENT

R.R and M.F acknowledge the Engineering and Physical Sciences Research Council (EPSRC), EU 7th framework small-scale collaborative project RESOLVE (NMP4-SL-2008-214340) and the University of Liverpool for grants and funding. M.P acknowledges the Swedish Research Council (VR) and the Marie Curie Research Training Network PRAIRIES, contract MRTN-CT-2006-035810. M.S.D acknowledges the University of Liverpool for funding of a postdoctoral fellowship and computational resources.

REFERENCES

(1) Ortega Lorenzo, M.; Baddeley, C. J.; Muryn, C.; Raval, R. *Nature* **2000**, *404*, 376.
(2) Perez Garcia, L.; Amabilino, D. *Chem. Soc. Rev.* **2007**, *36*, 941.
(3) Raval, R. *Chem. Soc. Rev.* **2009**, *38*, 707.
(4) Elemans, J. A. A. W.; de Cat, I.; Xu, H.; de Feyter, S. *Chem. Soc. Rev.* **2009**, *38*, 722.
(5) Barlow, S. M.; Raval, R. *Surf. Sci. Rep.* **2003**, *50*, 201.
(6) Barlow, S. M.; Raval, R. *Curr. Opin. Colloid Interface Sci.* **2008**, *13*, 65.
(7) Parikh, S. J.; Kubicki, J. D.; Jonsson, C. L.; Jonsson, C. M.; Hazen, R. M.; Sverjensky, D. A.; Sparks, D. L. *Langmuir* **2011**, *27*, 1778.
(8) Rankin, R. B.; Sholl, D. S. *J. Phys. Chem. B* **2005**, *109*, 16764.
(9) Rankin, R. B.; Sholl, D. S. *Surf. Sci.* **2004**, *548*, 301.
(10) Jones, G.; Jones, L. B.; Thibault-Starzyk, F.; Seddon, E. A.; Raval, R.; Jenkins, S. J.; Held, G. *Surf. Sci.* **2006**, *600*, 1924.
(11) Blanco-Rey, M.; Jones, G. *Phys. Rev. B.* **2010**, *81*, 205428.
(12) Fasel, R.; Wider, J.; Quitmann, C.; Ernst, K.-H.; Greber, T. *Angew. Chem., Int. Ed.* **2004**, *116*, 2913.
(13) Huang, T.; Hu, Z.; Wang, B.; Chen, L.; Zhao, A.; Wang, H.; Hou, J. G. *J. Phys. Chem. B* **2007**, *111*, 6973.
(14) Barbosa, L. A. M. M.; Sautet, P. *J. Am. Chem. Soc.* **2001**, *123*, 6639.
(15) Chen, W.; Li, H.; Huang, H.; Fu, Y.; Zhang, H. L.; Ma, J.; Wee, A. T. S. *J. Am. Chem. Soc.* **2008**, *130*, 12285.
(16) Bohringer, M.; Morgenstern, K.; Schneider, W.-D.; Berndt, R. *Angew. Chem., Int. Ed.* **1999**, *38*, 821.
(17) Bombis, C.; Weigelt, S.; Knudsen, M. M.; Nørgaard, M.; Busse, C.; Lægsgaard, E.; Besenbacher, F.; Gothelf, K. V.; Linderoth, T. R. *ACS Nano* **2010**, *4*, 297.
(18) Mark, A. G.; Forster, M.; Raval, R. *ChemPhysChem* **2011**, *12*, 1474.
(19) Forster, M.; Dyer, M. S.; Persson, M.; Raval, R. *J. Am. Chem. Soc.* **2009**, *131*, 10173.
(20) Lingenfelder, M.; Tomba, G.; Costantini, G.; Ciacchi, L. C.; De Vita, A.; Kern, K. *Angew. Chem., Int. Ed.* **2007**, *46*, 4492.
(21) Forster, M.; Dyer, M. S.; Persson, M.; Raval, R. *Angew. Chem., Int. Ed.* **2010**, *49*, 2344.
(22) Chen, Q.; Richardson, N. V. *Nat. Mater.* **2003**, *2*, 324.
(23) Goa, F.; Wang, Y.; Burkholder, L.; Tysoe, W. T. *Surf. Sci.* **2007**, *601*, 3579.
(24) Kuhnle, A.; Linderoth, T. R.; Hammer, B.; Besenbacher, F. *Nature* **2002**, *415*, 891.
(25) Kuhnle, A.; Linderoth, T. R.; Besenbacher, F. *J. Am. Chem. Soc.* **2003**, *125*, 14680.
(26) Eralp, T.; Shavorskiy, A.; Zheleva, Z. V.; Held, G.; Kalashnyk, N.; Ning, Y.; Linderoth, T. R. *Langmuir* **2010**, *26*, 18841.
(27) Smerieri, M.; Vattuone, L.; Costa, D.; Tielens, F.; Savio, L. *Langmuir* **2010**, *26*, 7208.
(28) Reichert, J.; Schiffrin, A.; Auwarter, W.; Weber-Bargioni, A.; Marschall, M.; Dell'Angela, M.; Cvetko, D.; Bavdek, G.; Cossaro, A.; Morgante, A.; Barth, J. V. *ACS Nano* **2010**, *4*, 1218.
(29) Barlow, S. M.; Kitching, K. J.; Haq, S.; Richardson, N. V. *Surf. Sci.* **1998**, *401*, 322.
(30) Booth, N. A.; Woodruff, D. P.; Schaff, O.; Giessel, T.; Lindsay, R.; Baumgartel, P.; Bradshaw, A. M. *Surf. Sci.* **1998**, *397*, 258.
(31) Kang, J.-H.; Toomes, R. L.; Polcik, M.; Kittel, M.; Hoeft, J.-T.; Efstathiou, V.; Woodruff, D. P.; Bradshaw, A. M. *J. Chem. Phys.* **2003**, *118*, 6059.
(32) Barlow, S. M.; Louafi, S.; Le Roux, D.; Williams, J.; Muryn, C.; Haq, S.; Raval, R. *Surf. Sci.* **2005**, *590*, 243.
(33) Barlow, S. M.; Louafi, S.; Le Roux, D.; Williams, J.; Muryn, C.; Haq, S.; Raval, R. *Surf. Sci.* **2005**, *590*, 243.
(34) Sayago, D. I.; Polcik, M.; Nisbet, G.; Lamont, C. L. A.; Woodruff, D. P. *Surf. Sci.* **2005**, *590*, 76.
(35) Haq, S.; Massey, A.; Moslemzadeh, N.; Robin, A.; Barlow, S. M.; Raval, R. *Langmuir* **2007**, *23*, 10694.
(36) Williams, J.; Haq, S.; Raval, R. *Surf. Sci.* **1996**, *368*, 303.
(37) Mateo Marti, E.; Barlow, S. M.; Haq, S.; Raval, R. *Surf. Sci.* **2002**, *501*, 191.
(38) Zhao, X.; Yan, H.; Zhao, R. G.; Yang, W. S. *Langmuir* **2003**, *19*, 809.
(39) Humblot, V.; Mthivier, C.; Pradier, C. M. *Langmuir* **2006**, *22*, 3089.
(40) Zhao, X.; Gai, Z.; Zhao, R. G.; Yang, W. S.; Sakurai, T. *Surf. Sci.* **1999**, *424*, L347.
(41) Zhao, X.; Zhao, R. G.; Yang, W. S. *Surf. Sci.* **1999**, *442*, L995.
(42) Iwai, H.; Tobisawa, M.; Emori, A.; Egawa, C. *Surf. Sci.* **2005**, *574*, 214.
(43) Jones, T. E.; Baddeley, C. J.; Gerbi, A.; Savio, L.; Rocca, M.; Vattuone, L. *Langmuir* **2005**, *21*, 9468.
(44) Feyer, V.; Plekan, O.; Skala, T.; Chab, V.; Matolin, V.; Prince, K. *J. Phys. Chem. B* **2008**, *112*, 13655.
(45) Cao, Y. W. C.; Jin, R.; Mirkin, C. A. *Science* **2002**, *297*, 1536.
(46) Izumi, Y. *Adv. Catal.* **1983**, *32*, 215.
(47) Schiffrin, A.; Riemann, A.; Auwarter, W.; Pannec, Y.; Weber-Bargioni, A.; Cvetko, D.; Cossaro, A.; Morgante, A.; Barth, J. V. *Proc. Natl. Acad. Sci. U.S.A.* **2007**, *104*, 5279.
(48) Bumm, L. A.; Arnold, J. J.; Cygan, M. T.; Dunbar, T. D.; Burgin, T. P.; Jones, L., II; Allara, D. L.; Tour, J. M.; Weiss, P. S. *Science* **1996**, *271*, 1705.
(49) Gautier, C.; Burgi, T. *J. Am. Chem. Soc.* **2006**, *128*, 11079.
(50) Gautier, C.; Burgi, T. *J. Am. Chem. Soc.* **2008**, *130*, 7077.

(51) Noguez, C.; Garzon, I. L. *Chem. Soc. Rev.* **2009**, *38*, 757.
(52) Sanchez-Castillo, A.; Noguez, C.; Garzon, I. L. *J. Am. Chem. Soc.* **2010**, *132*, 1504.
(53) Unac, R. C.; Gil Rabaza, A. V.; Vidales, A. M.; Zgrablich, G. *Appl. Surf. Sci.* **2007**, *254*, 125.
(54) Liu, N.; Haq, S.; Darling, G. R.; Raval, R. *Angew. Chem., Int. Ed.* **2007**, *46*, 1.
(55) Kresse, G.; Furthmüller, J. *Phys. Rev. B* **1996**, *54*, 11169.
(56) Kresse, G.; Joubert, J. *Phys. Rev. B* **1999**, *59*, 1758.
(57) Perdew, P.; Chevary, J. A.; Vosko, S. H.; Jackson, K. A.; Pederson, M. R.; Singh, D. J.; Fiolhais, C. *Phys. Rev. B* **1992**, *46*, 6671.
(58) Tersoff, J.; Hamann, D. R. *Phys. Rev. Lett.* **1983**, *50*, 1998.
(59) Riley, K. E.; Op't Holt, B. T.; Merz, K. M. *J. Chem. Theory Comput.* **2007**, *3*, 407.
(60) Itoh, K.; Kiyohara, T.; Shinohara, H.; Ohe, C.; Kawamura, Y.; Nakai, H. *J. Phys. Chem. B* **2002**, *106*, 10714.
(61) Bernardo, C. C. P. M.; Gomes, J. A. N. F. *J. Mol. Struct. (THEOCHEM)* **2002**, *582*, 159.
(62) Desiraju, G. R.; Steiner, T. *The Weak Hydrogen Bond*; Oxford University Press: New York, 1999.